Intriguing Prospects of a Novel Magnetic Nanohybrid Material: Ferromagnetic Fe-Rh Nanoparticles Grown on Nanodiamonds

Panagiotis Ziogas [1], Athanasios B. Bourlinos [1], Polyxeni Chatzopoulou [2], George P. Dimitrakopulos [2], Thomas Kehagias [2], Anastasios Markou [3] and Alexios P. Douvalis [1,4]*

[1] Physics Department, University of Ioannina, 45110 Ioannina, Greece
[2] Physics Department, Aristotle University of Thessaloniki, 54124 Thessaloniki, Greece
[3] Department of Solid State Chemistry, Max Planck Institute for Chemical Physics of Solids, 01187 Dresden, Germany
[4] Institute of Materials Science and Computing, University Research Center of Ioannina (URCI), 45110 Ioannina, Greece
* Correspondence: adouval@uoi.gr

Supplementary Materials (SM)

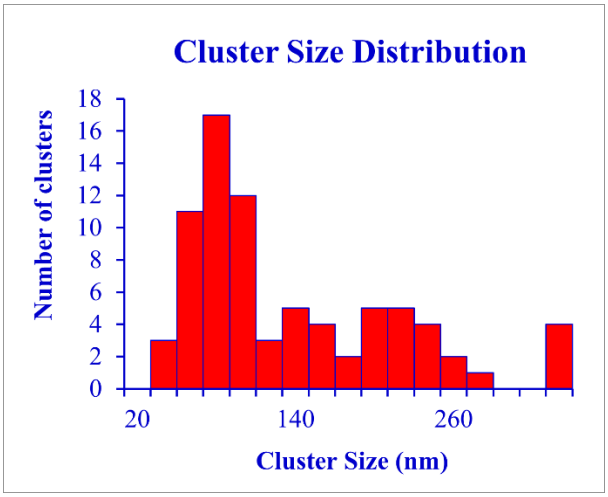

Figure S1. Histogram of the NDs' nanotemplate clusters size distribution appearing in the FeRh-AM-ND sample measured fromTEM.

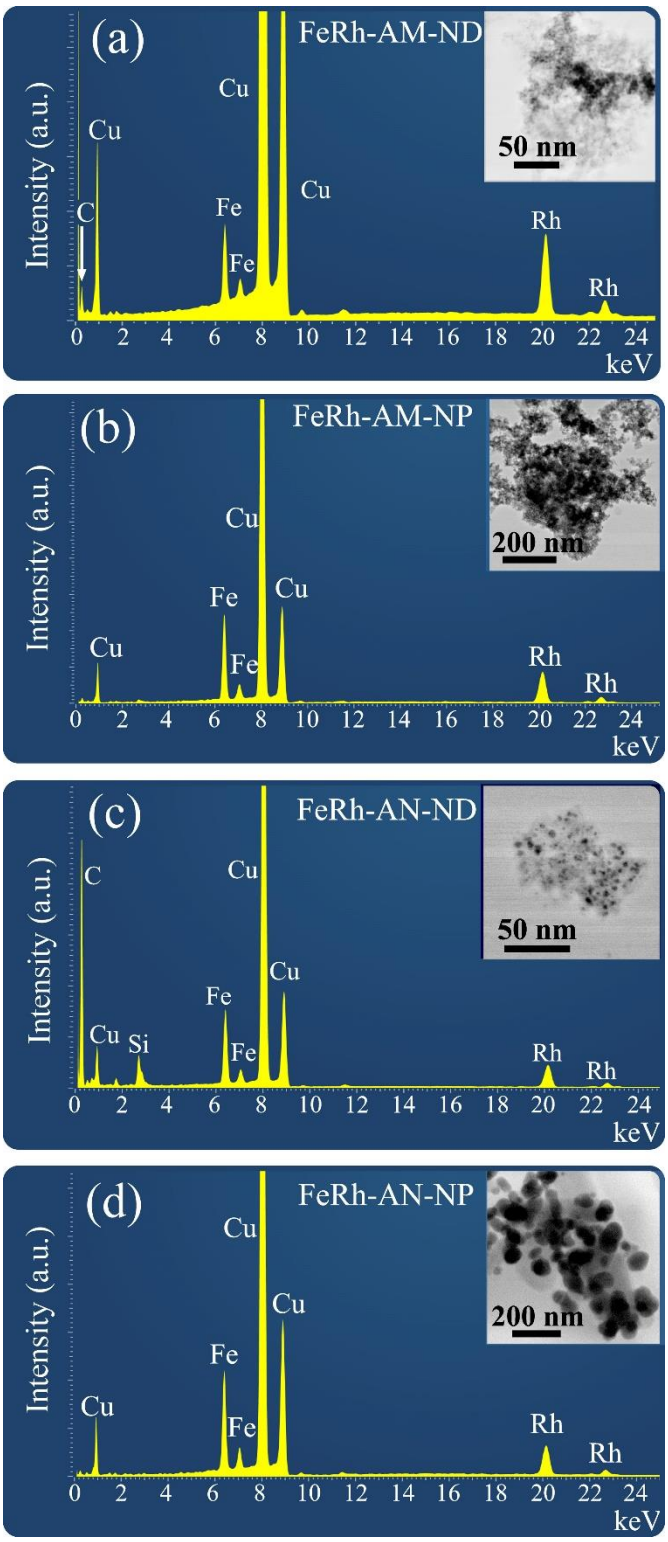

Figure S2. Overall EDS spectra, collected from the regions presented as insets. Sample tags are included in each spectrum. The Fe at% composition of the FeRh metallic alloys was calculated from the respective K_α peaks to be: before the annealing 10% in (a) and 23% in (b) and, after the annealing, 37% in (c), and 27% in (d). Cu peaks are due to the TEM supporting grids. In sample FeRh-AN-ND (c), the Si peak is attributed to contamination from the quartz ampule during the annealing.

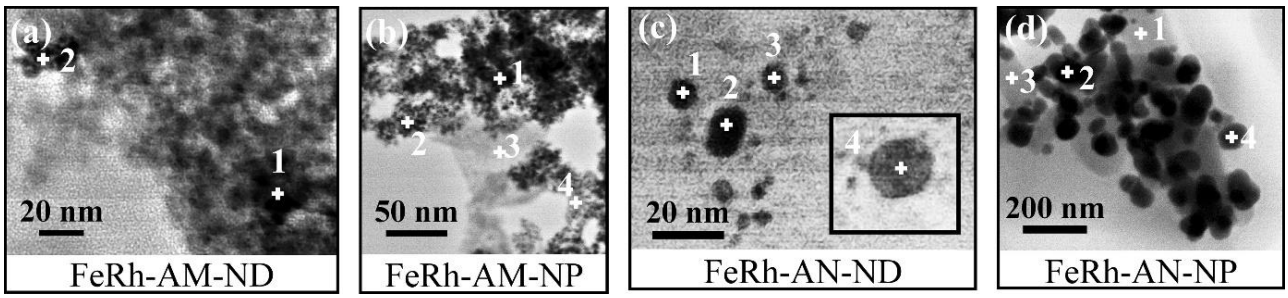

Figure S3. Indicative BF STEM images from all samples showing positions where EDS point analysis was performed. The corresponding measurements are given in Table S1.

Table S1. Fe at% composition (relative to Rh at%) of the FeRh metallic alloy calculated from the K_α peaks of point-spectra acquired from the points marked in Figure S3.

a. FeRh-AM-ND		b. FeRh-AM-NP		c. FeRh-AN-ND		d. FeRh-AN-NP	
Spot	**Fe %at**	**Spot**	**Fe %at**	**Spot**	**Fe %at**	**Spot**	**Fe %at**
1	23	1	9	1	22	1	100
2	12	2	14	2	23	2	17
		3	41	3	23	3	100
		4	15	4	29	4	8

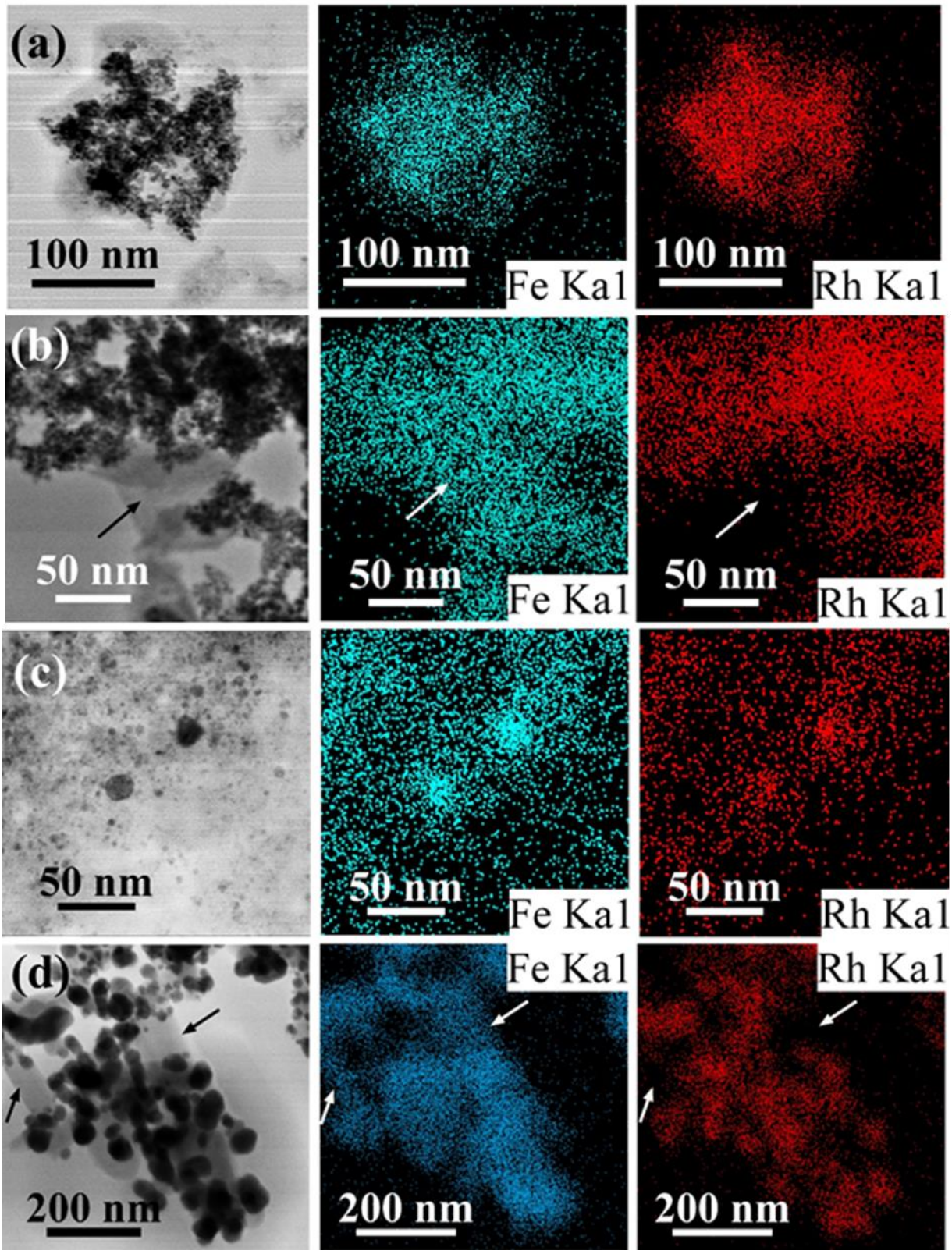

Figure S4. EDS Fe and Rh elemental maps obtained from samples (a) FeRh-AM-ND, (b) FeRh-AM-NP, (c) FeRh-AN-ND and (d) FeRh-AN-NP. Arrows in the unsupported free NP samples, i.e. (b) and (d), point at Fe-rich platelets, possibly connected to IOs and IOBs.

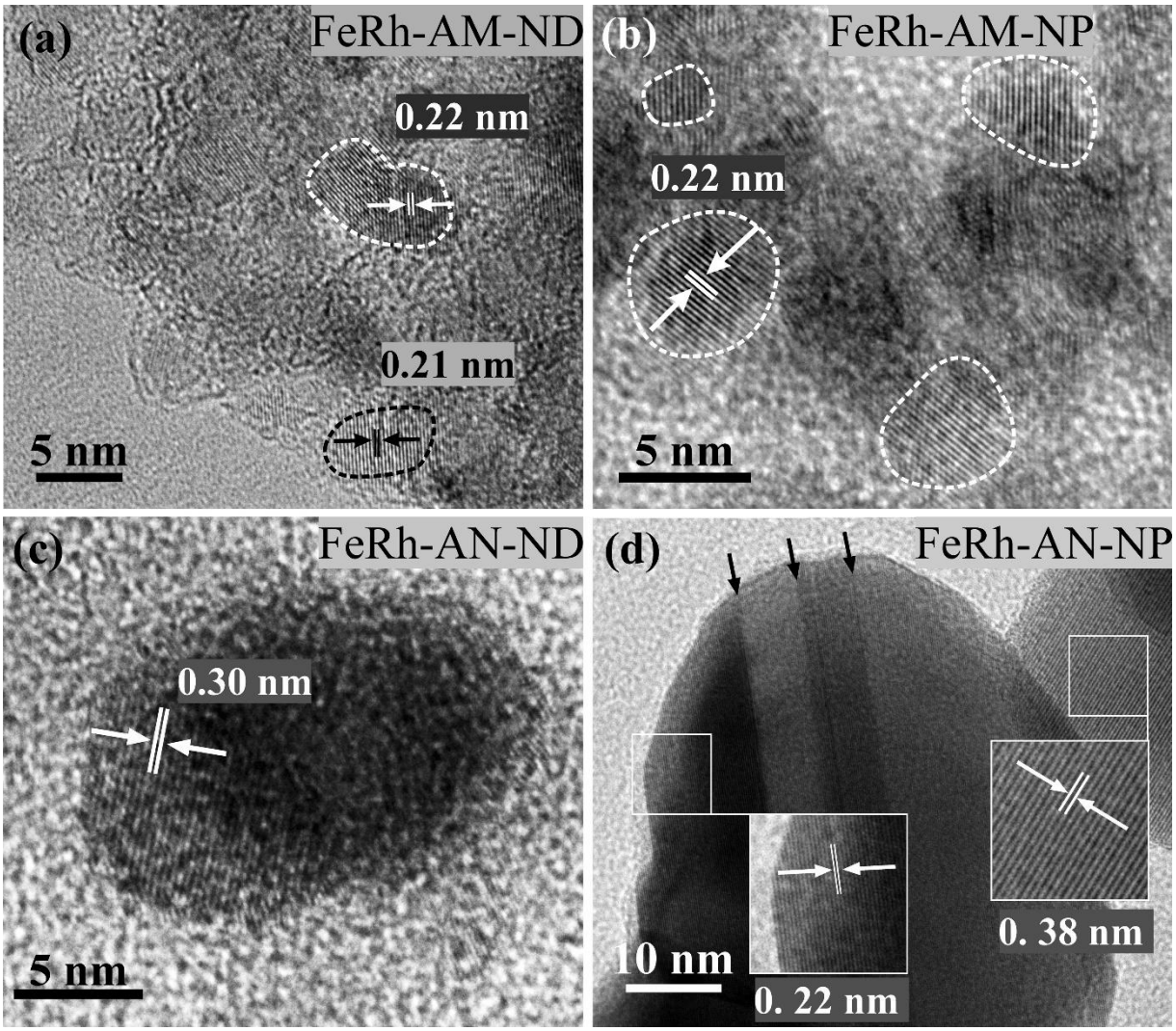

Figure S5. HRTEM images from samples (a) FeRh-AM-ND, (b) FeRh-AM-NP, (c) FeRh-AN-ND and (d) FeRh-AN-NP. In (a) and (b), {111}-lattice fringes measured at ~0.22 nm periodicity are shown in white, from fcc elemental Rh or Rh-rich γ-FeRh alloy NPs. In (a), ND {111}-lattice fringes with similar periodicity are shown in black (due to their similar {111} d-spacing, NPs and NDs are differentiated based on absorption contrast). In (c), {100}-lattice fringes of the CsCl-type α'-FeRh phase of a metallic NP after the annealing process, with ~0.30 nm spacing, are illustrated. In (d), Fe-Rh {111}- lattice fringes with spacing ~0.22 nm are measured in a spherical NP that exhibits twinning (black arrows), as well as lattice fringes of ~0.38 nm spacing in another NP, attributed to the {220} planes of iron oxyborate Fe_3BO_5.

Note: In NPs commonly their close-packed planes are resolved by HRTEM. In this case, the interplanar *d*-spacing of such planes are: For the {111} planes of ND, $d_{\{111\}\text{-ND}}$ = 0.206 nm, for the {111} planes of the FeRh fcc metallic phase $d_{\{111\}\text{-FCC}}$ = 0.216 nm, and for the {110} planes of the bcc phase $d_{\{110\}\text{-BCC}}$ = 0.212 nm. The close-packed planes of the metallic fcc and bcc phases are hardly discriminated within the spatial resolution of our camera. As a result, the bcc phase can only become discriminated if such a NP is oriented so that other crystal planes are diffracting that are characteristic of the bcc phase only. Since only the {100} and the {110} planes of this phase have *d*-spacings greater than the resolution limit of our microscope, the {100} planes are the only other choice. Hence, we illustrated in Fig. S5(c) an image of a NP with {100} planes (nominal *d*-spacing 0.2993 nm). Such a *d*-spacing does not exist in either the ND or the FCC phase.

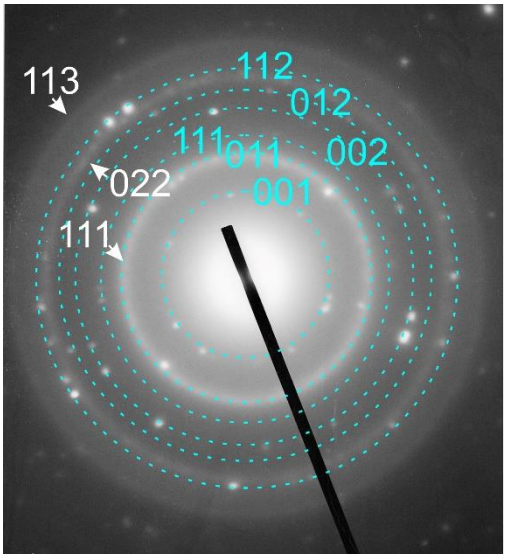

Figure S6. Electron diffraction pattern obtained from an area comprising larger NPs in sample FeRh-AN-ND. Arrows and white letters denote the Miller indices of rings from nanodiamond. Cyan letters and dashed circles denote respectively Miller indices and corresponding locations of reflections coming from the bcc α'-FeRh phase.

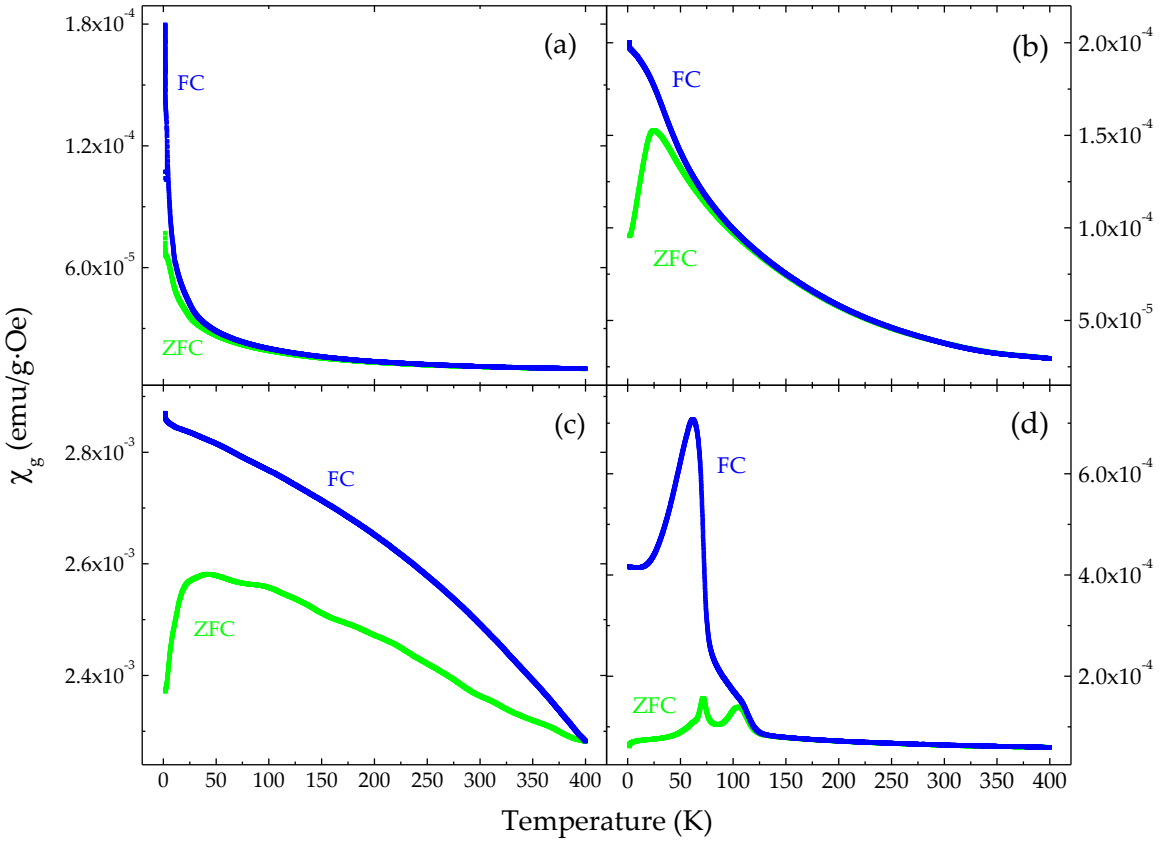

Figure S7. Mass magnetic susceptibility versus temperature measurements of the FeRh-AM-ND (a), FeRh-AM-NP (b), FeRh-AN-ND (c) and FeRh-AN-NP (d) samples measured under an applied external magnetic field of 999 Oe following ZFC (green) and FC (blue) modes.

Table S2. Mössbauer hyperfine parameters as resulting from the best fits of the corresponding spectra of the samples recorded at 77 K and 11 K. IS is the isomer shift (given relative to α-Fe at 300 K), Γ/2 is the half line-width, QS is the quadrupole splitting, 2ε is the quadrupole shift, B_{hf} is the hyperfine magnetic field, ΔQS is the spreading of QS and ΔB_{hf} is the spreading of B_{hf} around the central $QS^{(C)}$ or $Bhf^{(C)}$ values respectively (when these parameters are used) and AA is the relative spectral absorption area of each component used to fit the spectra. Typical errors are ± 0.02 mm/s for IS, Γ/2, 2ε and QS, ±3 kOe for B_{hf} and ± 5% for AA. In the cases where two ΔB_{hf} values are given, they correspond to asymmetric spreading around (lower/higher) the $Bhf^{(C)}$ value.

T K	Sample	IS mm/s	Γ/2 mm/s	$QS^{(C)}$ or 2ε mm/s	$B_{hf}^{(C)}$ kOe	ΔB_{hf} or ΔQS (kOe or mm/s)	AA %	Site - Phase	Color
77	FeRh-AM-ND	0.47	0.22	0.88	0	0.23	100	Fe^{3+} - IO/IHO (SPM)	Black
	FeRh-AM-NP	0.48	0.22	0.89	0	0.25	100	Fe^{3+} - IO/IHO (SPM)	Black
	FeRh-AN-ND	0.03	0.14	-0.02	273	0	45	Fe - bcc B2 α'-FeRh	Blue
		0.03	0.14	0.00	0	0	4	Fe - bcc B2 α'-FeRh (SPM)	Cyan
		0.38	0.35	0.76	0	0	51	Fe^{3+} - IO/IHO (SPM)	Red
	FeRh-AN-NP	0.23	0.22	0.00	0	0	27	Fe - fcc FeRh	Orange
		1.23	0.19	2.22	0	0	10	Fe^{2+} - Fe_3BO_5	Olive
		1.30	0.19	3.03	0	0	11	Fe^{2+} - Fe_3BO_6	Olive
		0.66	0.17	0.91	0	0	3	$Fe^{2.v+}$ - Fe_3BO_7	Olive
		1.23	0.19	2.19	47	0	20	Fe^{2+} - Fe_3BO_5	Olive
		0.52	0.19	0.82	323	0	10	Fe^{3+} - Fe_3BO_5	Olive
		0.87	0.19	1.36	347	0	9	$Fe^{2.5+}$ - Fe_3BO_5	Olive
		0.81	0.19	1.12	399	0	10	$Fe^{2.5+}$ - Fe_3BO_5	Olive
11	FeRh-AM-ND	0.47	0.20	0.90	0	0	49	Fe^{3+} - IO/IHO (SPM)	Red
		0.47	0.16	-0.01	487	17	7	Fe^{3+} - IO/IHO	Orange
		0.47	0.16	0.01	420	57	19	Fe^{3+} - IO/IHO	Magenta
		0.47	0.21	0.01	261	164	25	Fe^{3+} - IO/IHO	Brown
	FeRh-AM-NP	0.50	0.31	-0.03	488	12/4	30	Fe^{3+} - IO/IHO	Brown
		0.50	0.28	-0.03	449	24/6	50	Fe^{3+} - IO/IHO	Magenta
		0.50	0.14	-0.03	360	135/12	20	Fe^{3+} - IO/IHO	Orange
	FeRh-AN-ND	0.15	0.22	0.01	294	0	58	Fe - bcc B2 α'-FeRh	Blue
		0.15	0.17	0.00	0	0	4	Fe - bcc B2 α'-FeRh (SPM)	Cyan
		0.49	0.44	0.86	0	0	38	Fe^{3+} - IO/IHO (SPM)	Red
	FeRh-AN-NP	0.26	0.21	0.00	181	20	34	Fe - fcc FeRh	Orange
		1.24	0.17	2.10	94	0	7	Fe^{2+} - Fe_3BO_5	Olive
		1.24	0.17	2.15	249	0	10	Fe^{2+} - Fe_3BO_8	Olive
		1.24	0.17	2.15	205	0	5	Fe^{2+} - Fe_3BO_8	Olive
		1.31	0.31	3.03	161	0	11	Fe^{2+} - Fe_3BO_8	Olive
		0.53	0.17	0.82	491	0	10	Fe^{3+} - Fe_3BO_5	Olive
		0.82	0.17	1.14	515	0	5	$Fe^{2.5+}$ - Fe_3BO_5	Olive
		0.82	0.17	1.14	474	0	6	$Fe^{2.5+}$ - Fe_3BO_3	Olive
		0.88	0.17	1.36	432	0	6	$Fe^{2.5+}$ - Fe_3BO_4	Olive
		0.88	0.17	1.36	416	0	4	$Fe^{2.5+}$ - Fe_3BO_5	Olive
		0.69	0.17	0.93	414	0	2	$Fe^{2.v+}$ - Fe_3BO_5	Olive